Edge Steered Region Segmentation by Photometric Color Invariant

T. Gevers & A. W. M. Smeulders
Faculty of Mathematics & Computer Science, University of Amsterdam
Kruislaan 403, 1098 SJ Amsterdam, The Netherlands
E-mail: gevers@wins.uva.nl

Abstract

In this paper, an edge- and a region-based segmentation method are proposed effective for color images exploiting the change of apparent intensity independent of the viewpoint, the geometry of the object, the intensity and position of the illumination, and specularities (highlights).

Assuming dichromatic reflectance and white illumination, color models are identified denoting RGB-subspaces on which colors from the same shiny surface patch are projected under varying imaging conditions. The color invariant properties are then used to achieve robust photometric color invariant image segmentation.

To evaluate the performance of the segmentation methods, color images have been taken from full-color objects in real-world scenes where objects are composed of a variety of materials including plastic, textile, paper, wood, rubber, painted metal, ceramic and fruit.

Experiments show that the proposed segmentation methods are able to generate proper segmentation results independent of viewpoint of the camera, orientation of the object, direction and intensity of the illumination, and highlights.

The images and the performance of the segmentation methods can be experienced within the ZOMAX system on-line at http://www.wins.uva.nl/research/isis/zomax/.

1 Introduction

In this paper, the primary objective is to determine the image location where uniformly colored surface patches meet. In contrast to concentrating on a transition of color albedo, often referred to as material transition, it is common practice to concentrate on intensity transitions. As such, image segmentation is considered a statistical image processing problem of determining intensity edges in the presence of noise for example [2], [4]. However, intensity edges or region outlines may appear in the scene without a material transition to support it. In fact, intensity-based image segmentation methods cannot discriminate whether the intensity transition is due to material changes, shadows, abrupt surface orientation changes or highlights. Therefore, attention has been directed towards the use of color information. In the past, various color image segmentation methods have been proposed which do not account for the image formation process, [3], [12], [13], for example. A major drawback of the above color segmentation methods is that the values of the color features, on which the segmentation method relies, still depend on the geometry of the object, the viewpoint of the camera or the illumination conditions.

Color segmentation methods that account for the process of image formation are proposed recently. One of the first methods based on physics considerations is Klinker *et al.* [10]. They developed a clever color segmentation algorithm based on the dichromatic reflection model proposed by Shafer [16]. The method is based on evaluating "dog-leg" planar clusters in RGB-space. Then follows segmentation independent of the object's geometry, illumination conditions and highlights. To achieve robust image segmentation, however, surface patches of objects in view must have a rather broad distribution of surface normals which may not hold for objects in general. Bajscy *et al.* [1] developed a similar image segmentation method using the $H - S$ color space instead of the RGB-color space. Gevers and Groen [5], and Healey[7] propose different methods to segment images on the basis of normalized color. However, as normalized color is sensitive to highlights, a separate highlight removal technique is applied on the image prior to the actual segmentation. Furthermore, on the basis of physics considerations, Perez and Koch [15] prove that hue is a photometric color invariant to shading and highlights for a simple reflection model. On the basis of that consideration they use hue as the input for the actual segmentation algorithm.

From the arguments mentioned so far, it follows that the choice of color models is of great importance for the purpose of proper image segmentation. It induces the equivalence classes to the actual segmentation algorithm. The choice which color features to use depends on the imaging conditions.

To that end, in this paper, an edge- and a region-based segmentation method are proposed satisfying the following criteria: 1. Invariant to the viewpoint of the camera; 2. Invariant to the geometry of object in the scene being viewed; 3. Invariant to the intensity and position of the illumination; 4. Invariant to highlights.

In the paper, we assume dichromatic reflectance and white illumination. White illumination is not a severe restriction as one can usually control the lightning or color constant methods can be applied prior to the actual segmentation method. The RGB-subspace is identified satisfying the above criteria (i.e. being a photometric color invariant under the dichromatic reflection model) and evaluated for the purpose of color image segmentation in practice. In the evaluation, color images have been taken from full-color dielectric objects in real-world scenes where objects were composed of a large variety of materials including plastic, textile, paper, wood, rubber, painted metal, ceramic and fruit.

The paper is organized as follows. In Section 2, the dichromatic reflection model under white illumination is given. The reflection model is used to study and analyze the RGB- subspace on which colors will be projected from an uniformly painted surface patch. In Section 3, the edge steered region segmentation method is proposed.

2 Photometric Color Invariance

Consider an image of an infinitesimal surface patch. Using the red, green and blue sensors with spectral sensitivities given by $f_R(\lambda)$, $f_G(\lambda)$ and $f_B(\lambda)$ respectively, to obtain an image of the surface patch illuminated by a SPD of the incident light denoted by $e(\lambda)$, the measured sensor values will be given by Shafer [16]:

$$C = m_b(\vec{n}, \vec{s}) \int_\lambda f_C(\lambda) e(\lambda) c_b(\lambda) d\lambda + m_s(\vec{n}, \vec{s}, \vec{v}) \int_\lambda f_C(\lambda) e(\lambda) c_s(\lambda) d\lambda \tag{1}$$

for $C = \{R, G, B\}$ giving the Cth sensor response. Further, $c_b(\lambda)$ and $c_s(\lambda)$ are the albedo and Fresnel reflectance respectively. λ denotes the wavelength, $\vec{n}$ is the surface patch normal, $\vec{s}$ is the direction of the illumination source, and $\vec{v}$ is the direction of the viewer. Geometric terms m_b and m_s denote the geometric dependencies on the body and surface reflection respectively.

Considering dichromatic reflectance and "white" illumination, then $e(\lambda) = e$ and $c_s(\lambda) = c_s$. The measured sensor values are then [6]:

$$C_w = e m_b(\vec{n}, \vec{s}) k_C + e m_s(\vec{n}, \vec{s}, \vec{v}) c_s \int_\lambda f_C(\lambda) d\lambda \tag{2}$$

for $C_w \in \{R_w, G_w, B_w\}$ giving the red, green and blue sensor response under the assumption of a white light source. $k_C = \int_\lambda f_C(\lambda) c_b(\lambda) d\lambda$ is a compact formulation depending on the sensors and the surface albedo.

If the integrated white condition holds (as we assume throughout the paper):

$$\int_\lambda f_R(\lambda) d\lambda = \int_\lambda f_G(\lambda) d\lambda = \int_\lambda f_B(\lambda) d\lambda = f \tag{3}$$

we have:

$$C_w = C_b + C_s = e m_b(\vec{n}, \vec{s}) k_C + e m_s(\vec{n}, \vec{s}, \vec{v}) c_s f \tag{4}$$

2.1 Reflectance with White Illumination

In this paper, we concentrate on the following standard, **essentially different**, color features derived from RGB: intensity $I(R,G,B) = R + B + G$, RGB, normalized colors $r(R,G,B) = \frac{R}{R+G+B}$, $g(R,G,B) = \frac{G}{R+G+B}$, $b(R,G,B) = \frac{B}{R+G+B}$, hue $H(R,G,B) = \arctan(\frac{\sqrt{3}(G-B)}{(R-G)+(R-B)})$ and saturation $S(R,G,B) = 1 - \frac{\min(R,G,B)}{R+G+B}$.

For a given point on a shiny surface, the contribution of the body reflection component C_b and surface reflection component C_s are added together $C_w = C_b + C_s$. Hence, the observed colors of the surface will be inside the triangular color cluster in the RGB-space formed by the two reflection components [6], see Fig 1.a.

The triangular color cluster in the RGB-space forms a line-cluster in rgb-space, see Fig 1.a and 1.b, as can be seen as follows. Let P_d be the intersection of body color cluster vector $\vec{B}$ in RGB-sensor space. Then the chroma values of P_d are defined by:

$$\vec{p}_d = (\frac{e m_b(\vec{n}, \vec{s}) k_R}{e m_b(\vec{n}, \vec{s})(k_R + k_G + k_B)}, \frac{e m_b(\vec{n}, \vec{s}) k_G}{e m_b(\vec{n}, \vec{s})(k_R + k_G + k_B)}, \frac{e m_b(\vec{n}, \vec{s}) k_B}{e m_b(\vec{n}, \vec{s})(k_R + k_G + k_B)}) =$$

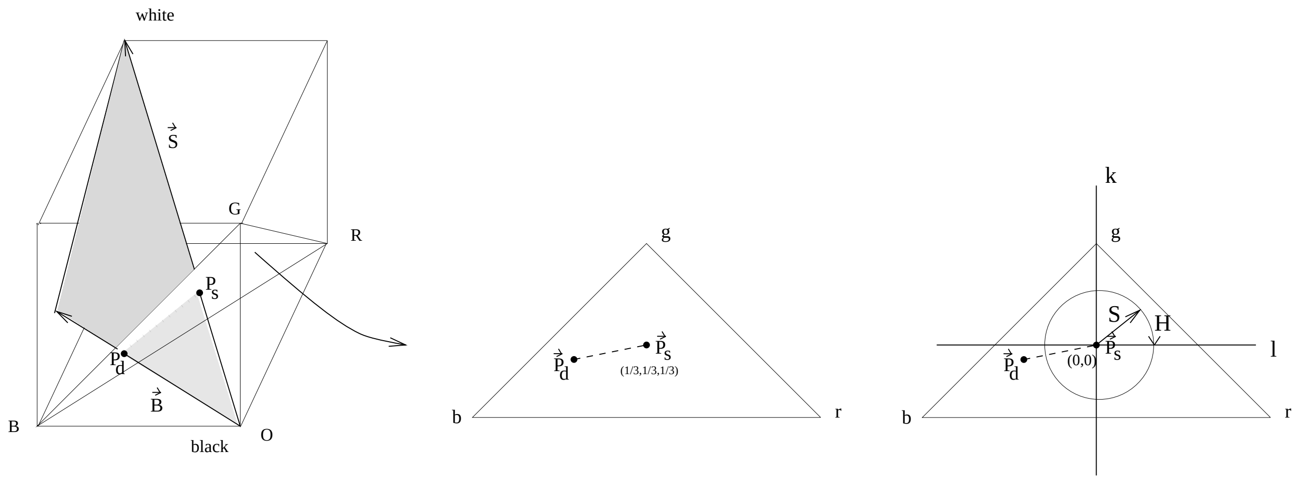

Figure 1: *a. Triangular color cluster $\vec{S}$ from a shiny uniformly colored surface in RGB. b. Projection of the triangular color cluster onto a line in the chromaticity plane originating at $(1/3, 1/3, 1/3)$. c. Saturation and hue defined in the kl-plane.*

$$\left(\frac{k_R}{k_R + k_G + k_B}, \frac{k_G}{k_R + k_G + k_B}, \frac{k_B}{k_R + k_G + k_B}\right) \tag{5}$$

Let P_s be the intersection of surface color cluster vector $\vec{S}$ with the unit plane. Then for the dichromatic reflection off an object illuminated with white light, we have:

$$\vec{p_s} = \left(\left(\frac{em_s(\vec{n}, \vec{s}, \vec{v})f}{3em_s(\vec{n}, \vec{s}, \vec{v})f}\right), \left(\frac{em_s(\vec{n}, \vec{s}, \vec{v})f}{3em_s(\vec{n}, \vec{s}, \vec{v})f}\right), \left(\frac{em_s(\vec{n}, \vec{s}, \vec{v})f}{3em_s(\vec{n}, \vec{s}, \vec{v})f}\right)\right) = (1/3, 1/3, 1/3) \tag{6}$$

That is, the reflection is also white.

Hence, $C_b + C_s$ is projected onto a line in the chromaticity originating at $\vec{p_s}$ and ending in $\vec{p_d}$, see Fig 1.b.

Now, we define the kl-plane to be the plane with origin at white point $(1/3, 1/3, 1/3)$ with the big advantage that hue and saturation are approximated by radial lines and concentric circles. Then, the observed color cluster of a shiny surface will be located in the kl-plane on a line of constant hue originating at the achromatic point $(0, 0)$. The definition of saturation and hue is graphically represented by Figure 1.c.

3 The Segmentation

To generate region outlines unaffected by the disturbing influences induced by the imaging process, the similarity criterion defined on a region should be true if pixels in that region have similar hue values. As we have deliberately defined an image invariant property, we aim at similarity matching where patches of similarity are steered by distinct edges in the invariant data field. However, unlike the other color features, hue is defined on a ring ranging $[0, 2\pi)$ instead of a linear *interval*. As a consequence, the hue values should be handled by a circular metric, before difference and similarity measures can be applied.

3.1 The Segmentation Algorithm

The segmentation algorithm we propose is an alternative of the split and merge procedure described in Horowitz and Pavlidis [8]. Instead of using quadtree-based image splitting, the splitting phase of our algorithm employs the incremental Delaunay triangulation competent of forming grid edges of arbitrary orientation and position.

A Delaunay triangulation $\mathcal{D}$ of a set of points V is a triangular tessellation of the plane in which the circumcircle of every triangle (v_i, v_j, v_k), where $v_i, v_j, v_k \in V$, does not contain in its interior any other point $v_l \in V$, [11] for example.

The tessellation grid is adjusted to the semantics of the image data by combining two basic, complementary information cues *similarity* and *difference*: if a global *similarity* criterion defined on a connected region is not satisfied, pixels of the heterogeneous region lying on image boundaries are determined using local *difference* measures and are used as new vertices to locally refine the tessellation grid.

The adaptive edge steered region segmentation is divided in three steps as follows:

Initialization: Let $\mathcal{D}^j$ denote the incremental Delaunay triangulation after j insertions of points in $\mathcal{N}^2$. Let d_i^j form the i^{th} triangle of the j^{th} triangulation. Further, consider the function $g : \mathcal{N}^2 \to \mathcal{N}^3$ defining a color image surface $g(x,y) = (R,G,B)$. $g_i^j(x,y)$ is a compact area of g which is bounded by the vertices of triangle d_i^j.

The image segmentation method starts with the construction of the initial triangulation $\mathcal{D}^0$ consisting of two triangles d_i^0 for $i = 1,2$ whose vertices are the corners of g.

Splitting: After the construction of $\mathcal{D}^0$, the algorithm successively examines triangles d_i^j by computing the similarity predicate $S()$. The similarity predicate is defined on g_i^j denoting the underlying image data of triangle d_i^j. If the similarity predicate is false, edge pixels in g_i^j are classified topographically based on their local neighborhood by the difference function $D()$. After edge detection, the most prominent point is selected and used as a vertex in $\mathcal{D}^j$ to generate the next triangulation $\mathcal{D}^{j+1}$ with the goal to adapt the image tessellation grid properly to the underlying structure of the image data. The splitting phase continues until all triangles satisfy $S()$. Edges of triangles typically coincide with (part of) a gradient stretch in the image.

Merging: Let R_i is a point set in $\mathcal{N}^2$ forming the i^{th} polygon with corresponding $r_i \subset \mathcal{N}^2$ a compact area of the plane by merging triangular areas of the final Delaunay triangulation ($\mathcal{D}^N$). In fact, $r_i = g_1^N \cup g_2^N \cup ... g_n^N$ where all n triangular image regions are adjacent.

The merging phase starts with the triangulation produced by the splitting phase $R_i = d_i^N$ for all i. Function $S()$ provides the criterion by which two adjacent polygons are merged into one. By using the same similarity predicate for the split- as well as the merge phase, the method, as a whole, will be robust against accidental splittings because accidental splittings will be recovered in the merge phase.

The quality of the algorithm is determined by functions $S()$ and $D()$. They are discussed in the following.

3.2 Similarity Predicate $S()$

We define region $\mathcal{R}$ to be homogeneous when the observed color cluster of the region can be approximated in the kl-plane by a line of constant hue originating at the achromatic point $(0,0)$. Hence, the similarity measure is based on fitting straight lines originating at $(0,0)$ in the kl-plane. If the mean fitting error is below a predefined threshold, region $\mathcal{R}$ is considered to be homogeneous. In this way, the similarity measure avoids the wrap-around nature of hue and is robust to pixels coming from the same uniformly painted surface patch but having very different saturation values due to highlights.

More formally, let $k(x,y)$ and $l(x,y)$ be the color coordinates k and l computed from RGB in the color image at location (x,y). A least-squares solver calculates the straight line parameter a originating at $(0,0)$ and the mean fitting error ϵ in the kl-plane by minimizing:

$$\epsilon = \sum_{\vec{x} \in \mathcal{R}} (l(\vec{x}) - ak(\vec{x}))^2 \tag{7}$$

over image region $\mathcal{R}$.

The mean noise standard deviation $\hat{\sigma}$ in the image is estimated by applying a least-squares fit to a uniformly colored region (in our case derived from a 5x5 mask).

Then, the similarity predicate $S()$, returning a Boolean value, is given by:

$$S(\mathcal{R}) = \begin{cases} \textit{true}, & \text{if } \epsilon \leq \hat{\sigma} \\ \textit{false}, & \text{otherwise} \end{cases} \tag{8}$$

defined over image region $\mathcal{R}$.

In other words, $\mathcal{R}$ is considered to be homogeneous if the colors of $\mathcal{R}$ form a line cluster, which falls within the limit of the mean image noise standard deviation, in the kl-plane originated at $(0,0)$.

3.3 Difference Measure $D()$

Due to the circular nature of hue, the standard difference operator is not suited for computing the difference between hue values. We define the difference between two hue values h_1 and h_2 as follows:

$$d(h_1, h_2) = \sqrt{(\cos h_1 - \cos h_2)^2 + (\sin h_1 - \sin h_2)^2} \tag{9}$$

yielding a difference $d(h_1, h_2) \in [0, 2]$ between h_1 and h_2.

To find hue edges in images we use an edge detector, currently of the Sobel type, where the component of the positive gradient vector in the x-direction is defined as follows:

$$H_x(\vec{x}) = \frac{1}{4}(d(H(x-1,y-1), H(x+1,y-1)) + 2d(H(x-1,y), H(x+1,y)) + d(H(x-1,y+1), H(x+1,y+1))) \tag{10}$$

where $H(\vec{x})$ denotes the hue value at image location $\vec{x}$. And in the y-direction as:

$$H_y(\vec{x}) = \frac{1}{4}(d(H(x-1,y-1), H(x+1,y-1)) + 2d(H(x,y-1), H(x,y+1)) + d(H(x-1,y+1), H(x+1,y+1))) \tag{11}$$

The gradient magnitude is represented by:

$$||\nabla H(\vec{x})|| = \sqrt{{H_x}^2 + {H_y}^2} \tag{12}$$

After computing the gradient magnitude, a non-maximum suppression process is applied to $||\nabla H(x,y)||$ in a standard way to obtain the local maxima in gradient values [2]:

$$\mathcal{M}(\vec{x}) = \begin{cases} ||\nabla H(\vec{x})||, & \text{if } (||\nabla H(\vec{x})|| > t_\sigma) \text{ is a local maximum} \\ 0, & \text{otherwise} \end{cases} \tag{13}$$

where t_σ is a threshold based on the noise level in the hue image to suppress marginally visible edges.

The hue gradient magnitude is pronounced strongest on hue edges since at these edges there is a relative strong change in hue values over a relative short distance. However, the hue gradient magnitude is less pronounced at corners. Because corners are topographically promising edge points to be inserted as vertices in the segmentation scheme, we adopt the curvature measure of [17] to be applied on the hue image:

$$\kappa(H) = H_{xx}H_y^2 - 2H_xH_{xy}H_y + H_x^2H_{yy} \tag{14}$$

where the partial derivatives take into account the circular nature of hue. The main advantage of using this curvature measure instead of the standard equation (defined as a change of gradient direction along an edge contour [9]) is that it detect edges, but its maximum value will be lying on a corner edge. The most prominent edge point to be inserted in the segmentation scheme, as described in Section 3.1, is defined as the point with maximum curvature magnitude.

4 The Experimental Setup

The images are taken from 3D full-color objects in real world scenes. The objects are composed of a large variety of materials such as fruit, paper, painted wood, textile, plastic and painted metal. Objects were recorded in 3 RGB-colors with the aid of the SONY XC-003P CCD color camera (3 chips) and the Matrox Magic Color frame grabber. The digitization was done in 8 bits per color. Objects were recorded against a cardboard background consisting of four uniformly painted rectangular areas. Two light sources of average day-light color are used to illuminate the objects in the scene. There was no attempt to individual control the focus or the illumination for the objects in the scene. Images show a considerable amount of noise, shadows, shading, specularities and inter-reflections. As a result, recordings are of as average quality, and a good representation of views from everyday life.

In the experiments, those pixels in a color image are discarded having a local absolute intensity and saturation smaller then 5 percent of the total range (this number was empirically determined by visual inspection); otherwise calculation of hue H, normalized colors rgb and saturation S become unstable. Consequently, dark or nearly colorless parts of objects or background as recorded in the color image will not be considered in the segmentation process.

The images and the performance of the segmentation methods can be experienced within the ZOMAX system on-line at http://www.wins.uva.nl/research/isis/zomax/.

5 Experiments

In this section, we evaluate and compare the performance of standard edge detection techniques [2] for the various color features, the new hue edge detector defined in Section 3.3 eq. (13), and the proposed edge steered region segmentation method according to the criteria given in Section 1.

The First Recording

Figure 3.a is an image of several toys against a background consisting of four squares. The size of the image is 256x256. The first upper left quadrant consists of three uniformly painted matte cubes of wood. The second upper right quadrant contains two specular plastic donuts on top of each other. In the bottom left quadrant a red highlighted ball and a matte cube are shown while the last quadrant contains two matte cubes. Note that each individual object is painted uniformly with a distinct color.

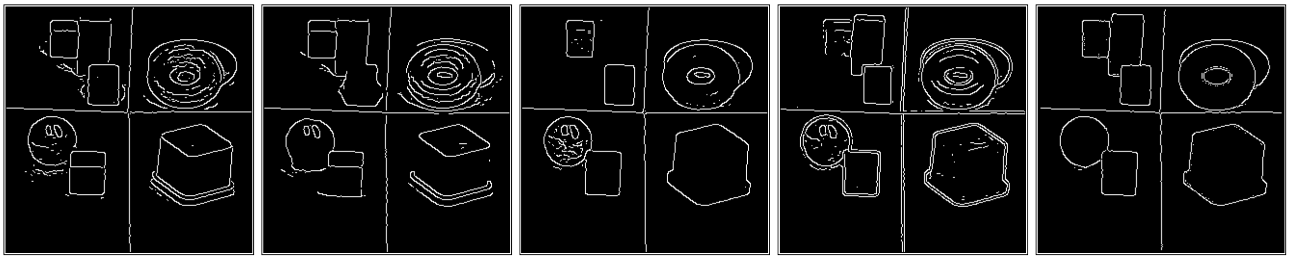

Figure 2: *Edge maps of the various color models computed from the first recorded color image shown in Figure 3.a. Standard edge detection is applied on the interval variables R, I, r and S images by Canny's edge detection algorithm with non-maximum suppression. The edge map of circular variable H is obtained by the developed hue-edge algorithm with non-maximum suppression. a. R-edge map. b. I-edge map. c. r-edge map. d. S-edge map. e. H-edge map. Note that only H produce edges corresponding to material transitions.*

Standard edge detection is performed on the interval variables R, I, r and S images by Canny's edge detection algorithm with non-maximum suppression. In Figure 2.a and 2.b edges are shown obtained from the R and I images respectively. Clearly, false edges are introduced by abrupt surface orientations, shadows, inter-reflections and highlights. In contrast, computed edges for r and S shown in Figure 2.c and 2.d respectively are insensitive for shadows and surface orientation changes but affected by inter-reflections (e.g. caused by the donuts and the background) and highlights (S more then r). In Figure 2.e the edge map is shown for circular variable H computed by the hue-edge algorithm defined in Section 3.3. Good performance is shown where computed edges correspond to material boundaries discounting the disturbing influences of surface orientation, illumination, shadows and highlights. Only inter-reflections disturb the quality of the edge map slightly (note that hue is not robust to inter-reflections). To avoid edges grouping to obtain proper regions outlines with closed contours, the hue edge map is used as an input of the region-based segmentation method.

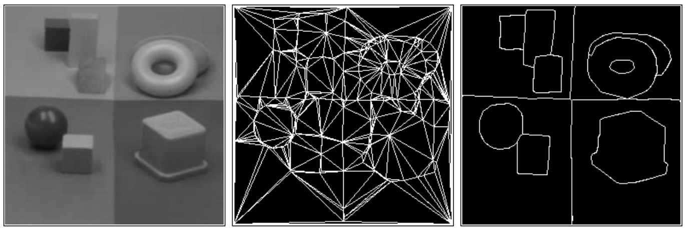

Figure 3: *a. First recorded color image. b. Splitting result of the split and merge method based on directed Delaunay splitting taken the hue-edge map shown in Figure 2.e on input. Note that proper conformation is established between tessellation grid and low-level image semantics. c. The final segmentation result of the region-based segmentation method. Note that the region outlines of the final result correspond neatly to material boundaries.*

In Figure 3.a the recorded color image is shown. The mean noise standard deviation is estimated by applying a least-squares fit to a uniformly colored region (5x5 mask). The measured mean noise standard deviation is $\hat{\sigma} = 3.1$ and used as the threshold for the similarity predicate $S()$. The splitting result is shown in Figure 3.b. Proper conformation is established between the tessellation grid and the low-level image semantics by the segmentation method based on directed Delaunay subdivision. The final segmentation result is shown in Figure 3.c. Despite the various radio-metrical and geometrical variations caused by the imaging process, region outlines correspond neatly to material boundaries. The computation of the hue edge map aside, total run time of the method took 14.5 seconds on a SPARC 10 station.

To evaluate and compare the quality of edge maps more objectively, the mean error distance is computed by applying the mean error distance on each of the edge maps with respect to the region outlines of the final segmentation result in Figure 3.c. The mean error distance for R, I, r S and H is respectively 3.6, 3.9, 1.7, 2.2 and 0.7. Obviously, H provides best edge map quality followed by r and S. The edge map quality of R and I are less in quality.

The Second Recording

In Figure 5.a, the second recorded full-color image is shown containing various rigid objects against a uniform background. The size of the image is 256x256. In the first quadrant, two cubes of painted wood are shown. The second quadrant contains a plastic cup and in the third quadrant a highlighted plastic donut is shown. The right-bottom quadrant consists of two cubes. Again, the image is affected by shadows, shading, highlights and inter-reflections. Each object is painted uniformly with a distinct color.

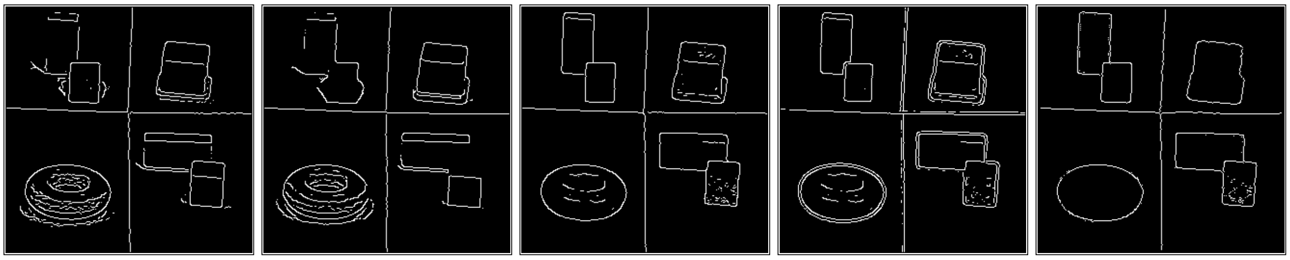

Figure 4: *Edge maps of various color models computed from the second recorded color image shown in Figure 5.a. a. R-edge map. b. I-edge map. c. r-edge map. d. S-edge map. e. H-edge map.*

In Figure 4, computed edges are shown obtained from the R, I, r and S images by the standard edge detection method and from the H image by the developed hue-based edge detection method. Falsely computed edges of R and I, depicted in Figure 4.a and 4.b respectively, are introduced due to shadows (e.g. casted by the cubes upon the background), abrupt surface orientation (e.g. the cup), inter-reflections (e.g. donut and background) and highlights (e.g. the highlighted donut). r and S yield edge maps fairly independent of shadows and abrupt surface orientation changes but erroneous edges are generated by image noise and small specularities due to local variations in material composition of objects and highlights. In contrast, good performance is shown for the hue-edge detector as depicted in 4.e.

The second recorded color image is shown in 5.a. The measured mean noise standard deviation is $\hat{\sigma} = 3.4$. The splitting result is shown in Figure 5.b. Good segmentation result is shown, in Figure 5.c, discounting the image noise and the radio-metrical imaging process. The run-time of applying the region-based segmentation method on the color image took 11.2 seconds user time on a SPARC 10 station.

The quality of the edge maps for the various color features is evaluated based on the mean error distance with respect to the segmentation result shown in Figure 5.c. The mean error distance for R, I, r S and H is respectively 4.9, 4.8, 2.7, 2.2 and 1.3. In conclusion, R and I provide bad edge map quality. r and S yields better results. Best quality is achieved by H.

6 Conclusion

In this paper, two methods have been proposed for color image segmentation. One is based on edge-segmentation, and an alternative is region-based employing directed Delaunay splitting. The purpose was to arrive at viewpoint invariant segmentation results, also insensitive to shadows, illumination intensity and surface reflection properties.

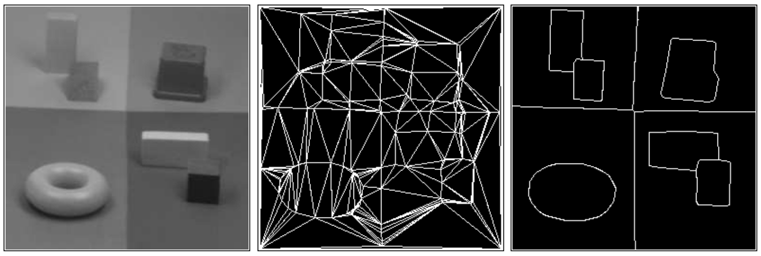

Figure 5: *a. Second recorded color image. b. Splitting result of the split and merge method based on directed Delaunay splitting taken the hue-edge map shown in Figure 4.e on input. c. The final segmentation result of the region-based segmentation method.*

From the experiments on man-made, full-color dielectric objects with a variety of surface textures, we can conclude that the proposed hue-edge detector provides material edges discounting the disturbing influences of surface orientation change, illumination, shadows and highlights. However, false edges are generated for very noisy homogeneous regions and minor inter-reflection cues. These disturbing influences are reduced using the hue-edge map as an input of the new region-based segmentation method. It yields a geometrically good and topologically sound segmentation result.

No constraints have been imposed on the images and the camera image process other than that images should be taken from chromatic dielectric objects illuminated by average day-light color. It is our point of view that these conditions are acceptable for a large variety of applications yielding a promising photometric color invariant image segmentation method.

References

[1] Bajcsy, R., Lee S. W., and Leonardis, A., *Color Image Segmentation with Detection of Highlights and Local Illumination Induced by Inter-reflections*, In IEEE 10th ICPR'90, pp. 785-790, Atlantic City, NJ, 1990.

[2] Canny, J., *A Computational Approach to Edge Detection*, IEEE PAMI, Vol. 8, No. 6, pp. 679-698, 1986.

[3] Celenk, M., *A Color Clustering Technique for Image Segmentation*, CVGIP, No. 52, pp. 145-170, 1990.

[4] Davis, L. S., *A Survey of Edge Detection Techniques* , CVGIP, Vol. 4, pp. 248-270, 1975.

[5] Gevers, T. and Groen, F. C. A., *Segmentation of Color Images*, In Proc. of 7th SCIA, Aalborg, 1991.

[6] Gevers, T. and Smeulders, A.W.M., *Object Recognition based on Photometric Color Invariants*, In Proc. of 10th SCIA, Lappeenranta, Finland, 1997.

[7] Healey, G., *Segmenting Images Using Normalized Color*, IEEE Syst., Man. Cybern., Vol. 22, pp. 64-73, 1992.

[8] Horowitz, S. L. and Pavlidis, T., *Picture Segmentation by a Directed Split-and-Merge Procedure* , In Proc. 2nd Int. Joint Conf. on Pattern Recog., Copenhagen, pp. 424-433, 1974.

[9] Kitchen, L. and Rosenfeld, A., *Gray-level corner detection*, PRL, 1, pp. 95-102, 1982.

[10] Klinker, G. J., Shafer, A. and Kanada, T. *A Physical Approach to Color Image Understanding*, Int. J. of Comp. Vision, Vol. 4, pp. 7-38, 1990.

[11] Lee, D. L. and Schachter, B. J., *Two Algorithms for Constructing a Delaunay Triangulation* , Int. J. of Comput. and Inf. Sc., Vol. 9, No. 3, pp. 219-424, 1980.

[12] Liu, J. and Yang, Y-H., *Multi-resolution Color Image Segmentation*, IEEE PAMI, Vol. 16, No. 7, pp. 689-700, 1994.

[13] Ohlander, R., *Analysis of Natural Scenes*, Ph.D. Thesis, Department of Computer Science, Carnegie-Mellon University, 1975.

[14] Ohta, Y., *Knowledge-Based Interpretation of Outdoor Natural Scenes*, Pitman Publishing, London, 1985.

[15] Perez, F. and Koch, C., *Towards Color Image Segmentation in Analog VLSI: Algorithm and Hardware*, Int. J. of Comp. Vision, Vol. 12, No. 1, pp. 17-42, 1994.

[16] Shafer, S. A., *Using Color to Separate Reflection Components*, COLOR Res. Appl., 10(4), pp 210-218, 1985.

[17] ter Haar Romeny, B. M., Florack, L, M., J., Koenderink, J. J., Viergever, M. A., *Invariant Third Order Properties of Isophotes: T-junction Detection*, In Proc. 7th SCIA, pp. 346-353, 1991.